Thrust Force Characteristics of Propulsion Mechanism in Fluid Using Variable-Bending-Stiffness Fin Modeled on Ciliary Movement*

Shunichi KOBAYASHI**, Tomoaki MASHIMA***
and Hirohisa MORIKAWA**

The application of dynamics observed in organisms is very instructive in the field of engineering. We noted the utility of ciliary movement for propulsion in fluid, and developed an enlarged propulsion mechanism modeled on ciliary movement. To realize the effective stroke and recovery stroke of ciliary movement, the mechanism was equipped with a motor on its base and a variable-bending-stiffness fin. The variable-bending-stiffness fin consists of two flexible sheets and electromagnets. Electromagnets control the frictional force between the two flexible sheets. Bending stiffness is controlled dynamically by changing the frictional force between the two flexible sheets. We discussed the thrust force characteristics of the mechanism in water and highly viscous liquid paraffin.

Key Words: Cilia, Ciliary Movement, Propulsion, Biomimetics, Biomechanics, Variable-Bending-Stiffness Fin

1. Introduction

Since most organisms are fairly autonomic, functional and efficient, the study of machines modeled on the movements of organisms is very significant in the engineering field. From this point of view, we aimed at examining the micropropulsion mechanism modeled on aquatic microorganisms. We have developed an enlarged propulsion mechanism modeled on eukaryotic flagellar movement[1],[2]. Microorganisms move in water by propulsion using not only flagellar movement but also ciliary movement. Ciliary movement has an advantage if the body is covered by many cilia such as in the case of a paramecium ; the body is able to rotate *in situ* and change its direction to propel itself in small spaces. Thus, we observed ciliary movement, and as the first step in the development of the propulsion mechanism modeled on ciliary movement, we fabricated an enlarged multilink mechanism in fluids[3]. This mechanism could realize the effective stroke and recovery stroke of ciliary movement, and works in low-Reynolds-number environments such as a highly viscous fluid. It is a new propulsion mechanism different from the screw propeller, particularly for use in highly viscous fluids. Furthermore, it can be an experimental simulator for micromachines and may contribute to the basic technical data for the design of micromachines in fluids for future use. However, this mechanism is heavy because it has three motors with high-reduction-gear-ratio units. To reduce the weight of the mechanism, we proposed the variable-bending-stiffness fin, which consists of two flexible sheets and an electromagnetic actuator. A similar study was conducted by Kawamura et al. who developed a variable-stiffness device[4],[5]. The device has a laminated structure of sheets and its stiffness is controlled by an electrostatic actuator and a pneumatic actuator. The principle of the mechanism is similar to that of a variable-bending-stiffness fin. However, we used an electromagnetic actuator to make the mechanism simpler than those of actuators. Furthermore, there is as yet no study of the variable-bending-stiffness fin for propulsion in fluids. Thus, the variable-bending-stiffness fin is a novel mechanism for propulsion in fluids.

The above mechanism is capable of changing the

* Received 29th May, 2003 (No. 03-4076)
** Department of Functional Machinery and Mechanics, Faculty of Textile Science and Technology, Shinshu University, 3-15-1 Tokida, Ueda, Nagano 386-8567, Japan. E-mail : shukoba@giptc.shinshu-u.ac.jp
*** Graduate School of Science and Technology, Shinshu University, 3-15-1 Tokida, Ueda, Nagano 386-8567, Japan

movement frequency, amplitude, and length of the fin, and working in water and highly viscous fluids. To determine the performance of this mechanism, we discussed the influence of these parameters on thrust force in water and highly viscous fluids.

2. Structure of Variable-Bending-Stiffness Fin

Figure 1 shows the structure of the variable-bending-stiffness fin. The fin consists of two flexible polypropylene sheets and three sets of electromagnets and steel disks. The flexible sheet is 0.2 mm thick. Three electromagnets are attached to one sheet, and three steel disks are attached to the other sheet at 20 mm intervals. The fin is connected to the drive shaft of the DC servomotor. Figure 2 shows a photograph of the variable-bending-stiffness fin in water. The bending stiffness of the fin was changed by controlling the sliding frictional force between the two flexible sheets explained as follows:

Low bending stiffness: The free sliding between the two sheets occurred due to the lack of electromagnetic force. The fin is bent by the drag force of water (Fig. 2(a)).

High bending stiffness: Two sheets are fixed by the electromagnetic force of excited electromagnets, and no sliding between the two sheets occurred. The fin is almost straight (Fig. 2(b)).

Figure 3 shows the schematic of an electromagnet. The iron core is made of electromagnetic soft iron. An enameled copper wire with a diameter of 0.1 mm was used as the coil, which was wound in 1 000 turns and had a resistance of 42 ohms. The excitation current for each electromagnet was set at 1.0 A.

For the evaluation of the bending stiffness of the fin, it would be best to use flexural rigidity EI, however, the fin was not made of a uniform material, and

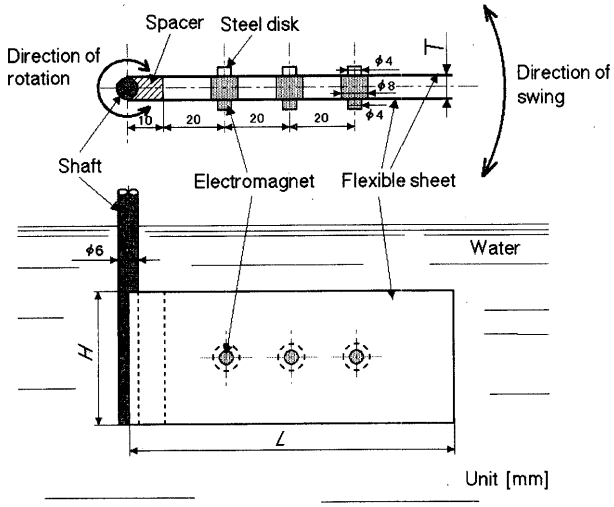

Fig. 1 Structure of variable-bending-stiffness fin

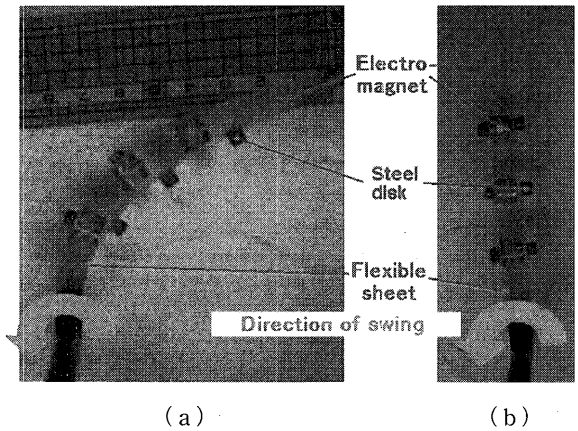

Fig. 2 Photograph of variable-bending-stiffness fin in water

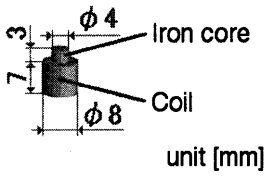

Fig. 3 Shematic of electromagnet

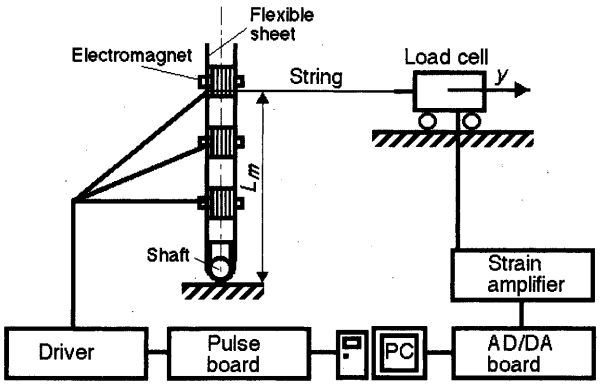

Fig. 4 Measurement system for fin's bending force and deflection

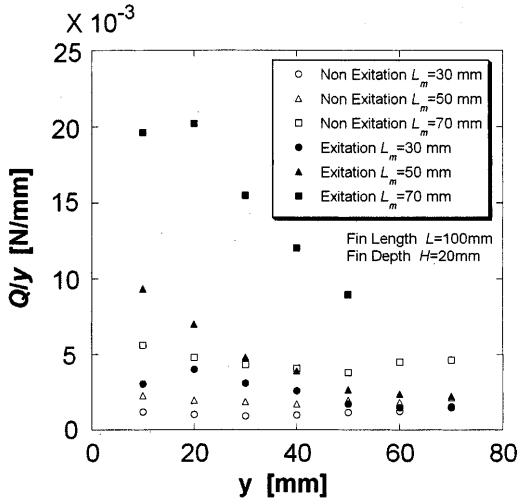

Fig. 5 Bending force per deflection of the fin

the bending curve was complex. Hence, we used bending force Q per deflection y as a simplified substitute parameter for bending stiffness. Figure 4 shows the measurement system for bending force and deflection. The rotating shaft was fixed and the fin was pulled using a string. The lateral force of the fin as bending force Q was measured using a load cell, and the distance that the load cell moved as deflection y was measured. The results are shown in Fig. 5. Bending force per deflection Q/y decreases with an increase in the deflection y, but the Q/y during excitation is much greater than that during no excitation.

3. Propulsion Mechanism in Fluid

3.1 Configuration of propulsion mechanism

Figure 6 shows a photograph of the propulsion mechanism. The variable-bending-stiffness fin is placed in water, and connected to the drive shaft from the DC servomotor (Maxon Motor, 11875). The DC servomotor consists of an encoder (Maxon Motor, HEDL5544) and a reduction gear (ratio 1 : 531, Maxon Motor, 114492).

3.2 Control and thrust force measurement of propulsion mechanism

Figure 7 shows the experimental system. The driving shaft connected to the DC servomotor is controlled by a personal computer (Hitachi Co. Ltd, PC-5DM02) through a servo driver (Maxon Motor, 4Q-DC, ADS50/S) and an AD/DA board (Interface Corp., IBX-3507). This control system can set the angular speed and maximum swing angle of the fin. The signals for the excitation of electromagnets are sent from a 128-channel pulse output board (Interface Corp., PCI-2426C) on a personal computer to the driver composed of a relay circuit (Omron Corp., G5V-2-12V).

The mechanism is able to move on the linear guide. During the measurement of x-directional thrust force (lateral force of the fin), the mechanism is connected to the load cell (NEC San-ei Instruments, T1). We confirmed that the error for the measurement of force along the linear guide was 0.001 N. The signal from the load cell is amplified by a strain amplifier and recorded on a personal computer in sync with the control of the DC servomotor.

3.3 Experimental conditions

Table 1 lists the experimental conditions. The general dimensions of the fin were based on the size and electromagnetic force of the electromagnets. To examine the influence of the length and width of the fin on thrust force characteristics, three fins of different dimensions were used. We used Fin B as the standard fin for the experiment. Movement frequency f and the maximum swing angle S, were changed. To discuss the influence of Reynolds number on thrust force characteristics, kinematic viscosity ν (working fluid) was also changed.

4. Results and Discussion

4.1 Shape of fin and variation of thrust force in one movement cycle

Figure 8 shows the change in fin shape (center line only, redrawn from photos) and variation of x-directional thrust force F_x for one movement cycle when F_x becomes cyclic. We defined positive thrust force

Table 1 Experimental conditions

Fin dimensions (Length: L, Depth: H, Thickness: T)	Fin A (L=100 mm, H=20 mm, T=7.4mm)
	Fin B (L=100 mm, H=40 mm, T=7.4mm)
	Fin C (L=160 mm, H=20 mm, T=7.4mm)
Number of electromagnets	3 (Fins A, B), 6 (Fin C)
Electric current on each electromagnet	1.0 A
Movement frequency: f	0.16 Hz – 0.5 Hz
Maximum swing angle: S	10 deg – 60 deg
Kinematic viscosity of working fluid: ν	1.00×10^{-6} m/s^2 (Water, 20 °C)
	1.51×10^{-3} m/s^2 (Liquid paraffin, 20 °C)

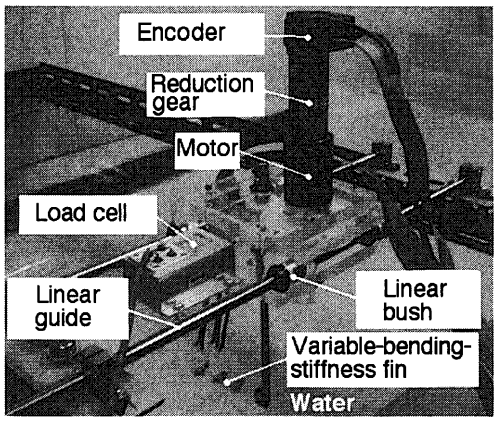

Fig. 6 Photograph of propulsion mechanism

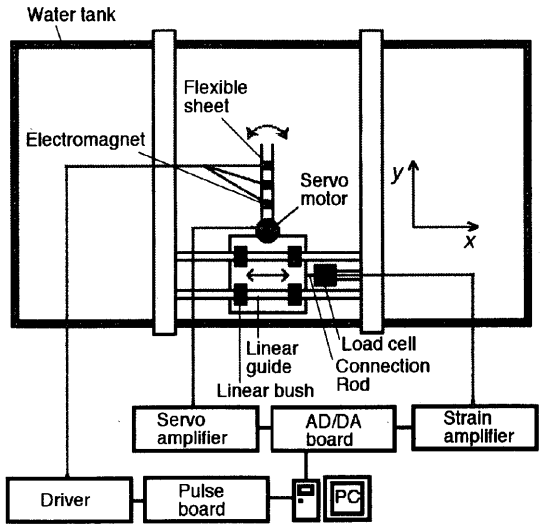

Fig. 7 Experimental system

for the negative direction of the x-axis shown in Fig. 7. The following three types of excitation pattern for the electromagnets were used to evaluate the effect of bending stiffness on fin shape and thrust force.

Type A: Excitation during the first half of the movement cycle (phase of 0 - 180 deg) and no excitation during the second half of the movement cycle (phase of 180 - 360 deg).

Type B: No excitation during whole movement cycle.

Type C: Excitation during whole movement cycle.

For Type A, the change in fin shape is similar to the ciliary movement: During the first half of the movement cycle, the fin is straight and the fin works in the effective stroke; during the second half of the movement cycle, the fin is bent by the drag force of water and works in the recovery stroke. The magnitude of thrust force during the effective stroke is higher than that during the recovery stroke. For Type B, the fin is bent during the whole movement cycle. The magnitude of thrust force during the first half of the movement cycle for Fin B is lower than those for Types A and C, and that during the second half of the movement cycle for Type B is almost the same as that for Type A. For Type C, fin does not bend during the whole movement cycle. The magnitude of thrust force during the second half of the movement cycle for Type C is larger than those for Types A and B. The average thrust forces in one movement cycle F_{xave} for Types A, B and C are 16.5×10^{-3} N, 7.0×10^{-3} N and 5.9×10^{-3} N, respectively, and the thrust force differences in one movement cycle ΔF_x ($=F_{x\max}-F_{x\min}$) for Types A, B and C are 0.18 N, 0.12 N and 0.25 N, respectively. Therefore, Type A is a good excitation pattern for a high average thrust force and a low thrust force difference.

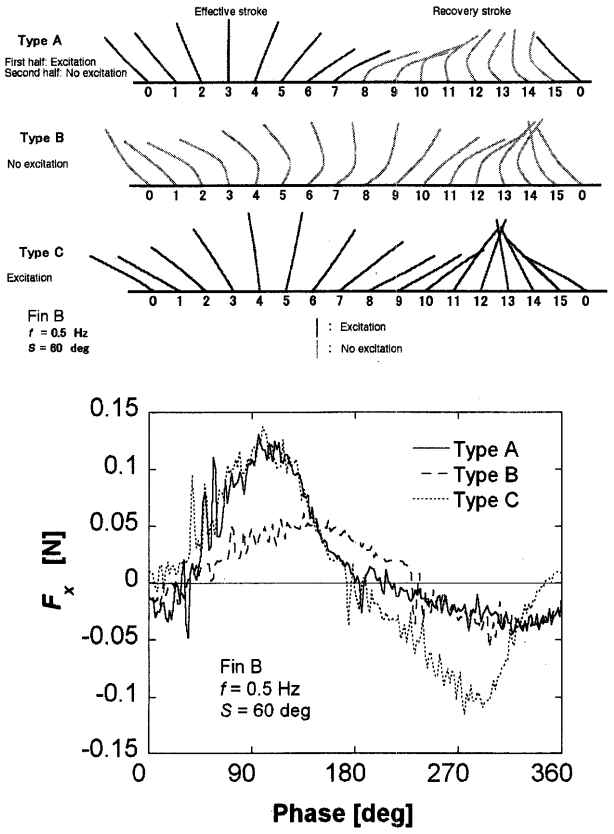

Fig. 8 Change in fin shape and variation of x-directional thrust force F_x for one movement cycle

4.2 Influence of movement frequency on thrust force

Figure 9 shows average thrust force F_{xave} and thrust force difference ΔF_x ($=F_{x\max}-F_{x\min}$) in one movement cycle versus movement frequency f. Average thrust force F_{xave} increases with an increase in f higher than 0.25 Hz. It is suggested that the fin does not bend at an f lower than 0.25 Hz, the magnitude of positive thrust force during the first half and that of negative thrust force during the second half were almost the same. Furthermore, the values of ΔF_x at f of 0.33 Hz and 0.5 Hz were almost the same, although the values of F_{xave} are different. This is caused by the fin's bending: since the fin during the recovery stroke at f of 0.5 Hz was bent greater than that at f of 0.33 Hz, the magnitude of thrust force during the recovery stroke at an f of 0.5 Hz was not greatly increased.

4.3 Influence of maximum swing angle on thrust force

Figure 10 shows average thrust force F_{xave} and thrust force difference ΔF_x ($=F_{x\max}-F_{x\min}$) in one movement cycle versus swing angle S. Average thrust force F_{xave} and thrust force difference ΔF_x increases with an increase in S. It is suggested that the drag force of water increases with increasing speed of the fin movement, and acts on the greater

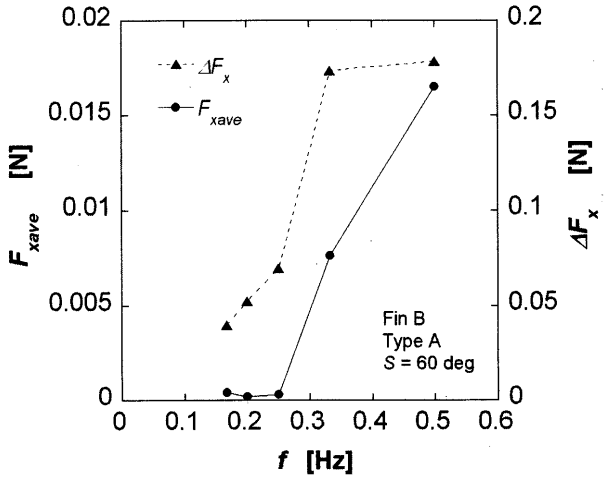

Fig. 9 Average thrust force F_{xave} and thrust force difference ΔF_x ($=F_{x\max}-F_{x\min}$) versus movement frequency f

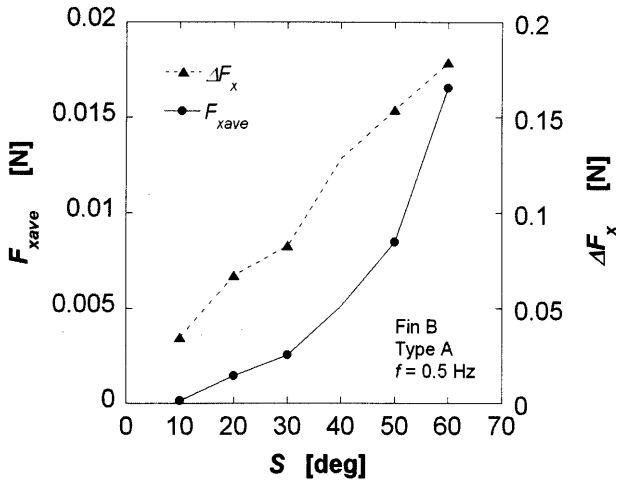

Fig. 10 Average thrust force F_{xave} and thrust force difference ΔF_x ($=F_{x\max}-F_{x\min}$) versus swing angle S

thrust force.

4.4 Influence of fin size on thrust force

Figure 11 shows the change in fin shape (center line only, redrawn from photos) and variation of x-directional thrust force F_x for one movement cycle for three fins of different sizes. The depth H of Fin A is one-half that of Fin B. The length L and number of electromagnets of Fin C are double those of Fins A and B. The average thrust forces F_{xave} of Fins A, B and C are 5.6×10^{-3} N, 16.5×10^{-3} N and 12.7×10^{-3} N, and the thrust force differences ΔF_x of Fins A, B and C are 0.09 N, 0.179 N and 0.10 N, respectively. The shape of Fin A is almost the same as that of Fin B; however, the magnitude of thrust force of Fin A is smaller than that of Fin B. This indicates that a larger depth is effective for increasing thrust force. Fin C during the first half of the movement cycle (excitation of all magnets) is not straight, and its average thrust force F_{xave} does not increase although its thrust force at around the end of the first half of the movement cycle (phase of 160 - 180 deg) is the greatest for the three fins. This is caused by the increased drag force of water that bent the long fin even when all the electromagnets were excited. Therefore, stiffer flexible sheets and electromagnets that generate greater force are necessary.

4.5 Influence of kinematic viscosity on thrust force

To reduce the Reynolds number of the mechanism, we used a highly viscous liquid paraffin. We defined Reynolds number Re as

$$Re=\frac{V_aH}{\nu}, \qquad (1)$$

where V_a is the average circumferential speed at the middle of the fin ($L/2$). For example, in the case of Fin A ($L=100$ mm) and $f=0.25$ Hz, $V_a=52.5$ mm/s.

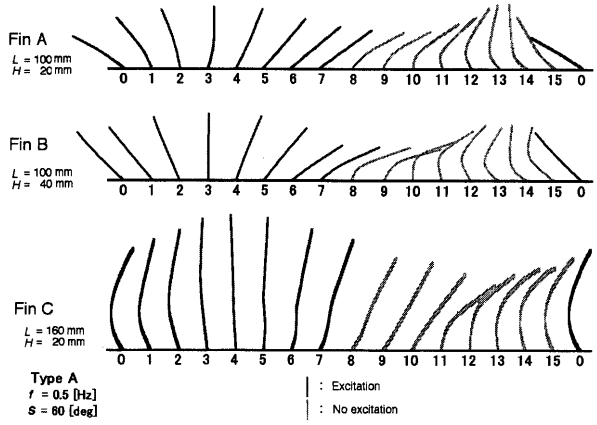

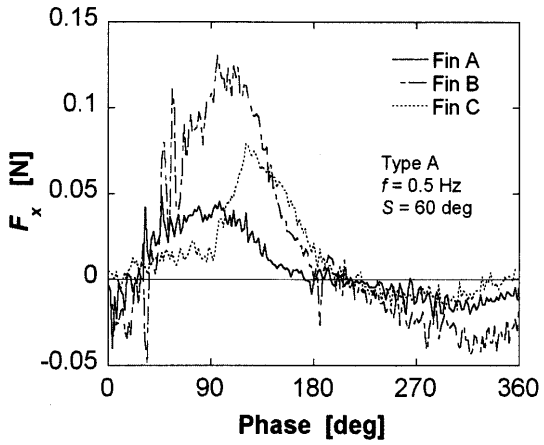

Fig. 11 Change in fin shape and variation of x-directional thrust force F_x for one movement cycle for the three fins of different sizes

ν is the kinematic viscosity of the working fluid. The Re values of water and liquid paraffin at $V_a=52.5$ mm/s are 2.1×10^3 and 1.4, respectively. Figure 12 shows the change in fin shape (center line only, redrawn from photos) and variation of x-directional thrust force F_x for one movement cycle for water and liquid paraffin. The average thrust forces F_{xave} for water and liquid paraffin are 0.3×10^{-3} N and 6.0×10^{-3} N, and the thrust force differences ΔF_x are 0.07 N and 0.14 N, respectively. F_{xave} for liquid paraffin is approximately 20 times greater than that for water; however, ΔF_x for liquid paraffin is approximately 2 times greater than that for water. This is explained as follows: (1) the greater the resistive force of the more viscous liquid paraffin, the greater the thrust force. (2) Since the fin in more viscous liquid paraffin is bent to a greater extent particularly during the recovery stroke, the negative thrust force during this stroke is not greater.

At an f of 0.5 Hz, the fin was bent to be a greater extent from the first half of the movement cycle, thus thrust force did not increase. With the inclusion of the results for the long fin (Fin C), a greater bending stiffness is required for the effective stroke; however,

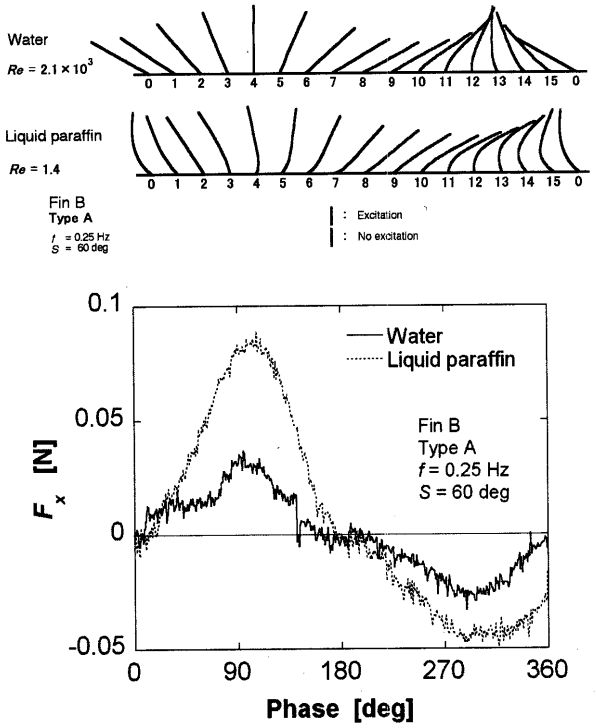

Fig. 12 Change in fin shape and variation of x-directional thrust force F_x for one movement cycle for water and liquid paraffin

at greater bending stiffness, fin does not bend during the second half of the cycle (no excitation) for low movement frequency and in water. Hence, a fin with wider range of bending stiffness is required.

The Reynolds number of the fin in liquid paraffin was considerably greater than that of the cilia in water, for example, $Re=1.1\times10^{-3}$ for the movement of a single large abfrontal cilium of Mytilus[6] in water (length$=$100 μm, diameter$=$10 μm, frequency$=$0.5 Hz, diameter is substituted for H in Eq.(1)). A smaller fin or a higher viscosity of fluid is required to simulate the ciliary movement of organisms in the future. Moreover, the development of a propulsion mechanism with many fins is necessary in the future.

5. Conclusions

This study was conducted to develop an enlarged propulsion mechanism in a fluid modeled on ciliary movement. For the fin of the mechanism, we developed a variable-bending-stiffness fin, which consists of two flexible sheets and an electromagnetic actuator. The following results were obtained:

(1) The fin realized the effective stroke and recovery stroke of ciliary movement in water and liquid paraffin.

(2) The average thrust force and thrust force difference in one movement cycle increased with an increase in frequency and maximum swing angle in water.

(3) The thrust force of a large-depth fin (Fin B) was greater than that of a small-depth fin (Fin A) in water.

(4) The longer fin (Fin C) bent during whole movement cycle in water.

(5) The average thrust force and thrust force difference in one movement cycle in liquid paraffin ($Re=1.4$) were 20 and 2 times greater, respectively, than those in water ($Re=2.1\times10^{3}$).

Acknowledgements

This work was supported by a research grant from the Fundamental Research Developing Association for Shipbuilding and Offshore, Grant-in-Aids for Scientific Research (13450096-01, 13650275-00) from the Japan Society for the Promotion of Science, and a Grant-in-Aid for the 21st Century COE Program by the Ministry of Education, Culture, Sports, Science, and Technology.

References

(1) Kobayashi, S., Furihata, K. and Morikawa, H., Propulsion Mechanism Modeled on Bending Mechanism of Eukaryotic Flagellar Bending in Water, Journal of Robotics and Mechatronics, Vol. 13, No. 1 (2001), pp. 96-100.

(2) Kobayashi, S., Furihata, K., Nakasone, M. and Morikawa, H., Thrust Force Characteristics of Propulsion Mechanism Modeled on Bending Mechanism of Eukaryotic Flagella in Water, JSME Int. J., Ser. C, Vol. 44, No. 4 (2001), pp. 946-951.

(3) Mashima, T., Kobayashi, S. and Morikawa, H., Multi-Link Mechanism Modeled on Ciliary Motion in Water, Proceedings of 2000 Annual Conference of JSME, Vol. VI, (in Japanese), (2000), pp. 133-134.

(4) Tabata, O., Kohishi, S., Cusin, P., Ito, Y., Kawai, F., Hirai, S. and Kawamura, S., Microfabricated Tunable Bending Stiffness Device, Proceedings of IEEE the 13th Annual International Conference on Micro Electro Mechanical Systems, (2000), pp. 23-27.

(5) Kawamura, S., Yamamoto, T., Ishida, D., Ogata, T., Nakayama, Y., Tabata, O. and Sugiyama, S., Development of Passive Elements with Variable Mechanical Impedance for Wearable Robots, Proceedings of 2002 IEEE International Conference on Robotics and Automation, (2002), pp. 11-15.

(6) Baba, S.A. and Hiramoto, Y., A Quantitative Analysis of Ciliary Movement by Means of High-Speed Microcinematography, Journal of Experimental Biology, Vol. 52 (1970), pp. 675-690.